Using System Identification to Compare Global and Local Aerodynamic Modeling from Flight Data

A Thesis Presented for the

Master of Science

Degree

The University of Tennessee, Knoxville

Toby Earl Sorensen

May 2013

Copyright © 2013 by Toby Earl Sorensen
All rights reserved.

DEDICATION

To my beautiful wife Savanna, my wonderful and fun kids; Gaige and Briel, and to our little baby on the way.

ACKNOWLEDGEMENTS

I would like to thank my family and friends for their support and encouragement throughout the pursuit of my Master of Science in Flight Test Engineering. I would especially like to thank Mr. Borja Martos for his patience, kindness, for all the time he has spent teaching me, his unwavering support and believing in me. Also, I would like to thank Devon Simons and Borja Martos for being the excellent test pilots who skillfully flew the flight test maneuvers. Also, a big thanks goes to Jonathan Kolwyck for his friendship, his help in proof reading over my drafts and for him talking about all the material with me; it helped me to learn it better. I would also like to thank Dr. Peter Solies and Dr. Trevor Moeller for serving as members on my thesis committee.

I owe a great deal of gratitude to my wife, Savanna, for her constant encouragement and patience in dealing with me being in school throughout our married life of 7 years. Last, but not least, I thank my children Gaige and Briel for understanding that I could not play with them as much; I will now be able to play with you more. This project would not have been possible without all of you. Thank you.

ABSTRACT

A method for identifying and comparing a longitudinal global aerodynamic model to a longitudinal local aerodynamic model for UTSI's Piper Saratoga aircraft is explained and demonstrated. Large amplitude piloted inputs were used to estimate global nonlinear aerodynamic models from flight data. Flight derived global aerodynamic model structures, model parameter estimates, and associated uncertainties were provided for the longitudinal dimensional force and moment. The results from the global aerodynamic modeling were compared to local linear aerodynamic modeling results gathered with traditional small amplitude doublet inputs. The results from large amplitude piloted inputs compared favorably with small amplitude piloted inputs by ten percent in almost all cases and in significantly less test time.

TABLE OF CONTENTS

Introduction 1
Chapter 1 Theoretical Background 3
1.1 Derivation of the Equations of Motion 3
1.2 System Identification 11
1.3 Converting Measured Data to the Frequency Domain 12
1.4 Estimating the Dimensional Stability and Control Derivatives using Equation-Error . 15
Chapter 2 Research Aircraft 17
2.1 Aircraft 17
2.2 Instrumentation 17
Chapter 3 Manerver Design 19
3.1 Maneuver Implementation 19
3.2 Small Amplitude Maneuvers for Local Aerodynamic Modeling 20
3.3 Large Amplitude Maneuvers for Global Aerodynamic Modeling 20
Chapter 4 Flight Test Results 22
Conclusions 30
References 31
Appendix 33
Tables 34
Derivation of the Equations of Motion from First Principles 36
Figures 39
Vita 40

LIST OF TABLES

Table 1. Small Amplitude Maneuvers Compared with Cut Data Sets from Large Amplitude Maneuver 34
Table 2. Stepwise regression results, body-axis Z force for a large amplitude maneuver 35
Table 3. Large Amplitude Maneuver Comparison Near and Through Stall..... 35

LIST OF FIGURES

Figure 1. Piper Saratoga, PA 32-301 17
Figure 2. Factory Installed ADS 18
Figure 3. Flight Test ADS 18
Figure 4. After Market Static Ports 18
Figure 5. Air Data Vanes 18
Figure 6. LabVIEW® Virtual Instrument Input Tones 20
Figure 7. Input Tones Implementation 20
Figure 8. Measured Time Series – Multiple Doublets at 100 KIAS 22
Figure 9. Body-Axis Z Force vs. Frequency – Multiple Doublets at 100 KIAS 23
Figure 10. Pitch Moment M vs. Frequency – Multiple Doublets at 100 KIAS 23
Figure 11. Measured Time Series – Longitudinal Large Amplitude Maneuver without Stall 24
Figure 12. Longitudinal Large Amplitude Maneuver Z vs. Frequency 25
Figure 13. Longitudinal Large Amplitude Maneuver M vs. Frequency 25
Figure 14. NACA 66_2-415 Airfoil Lift Curve Slope 26
Figure 15. Longitudinal Large Amplitude Maneuver Independent Variable Cross Plots 27
Figure 16. Measured Time Series – Longitudinal Large Amplitude Maneuver through Stall 28
Figure 17. Parameter Estimates Comparison 29
Figure 18. Chirp Z Transform Diagram[8] 39
Figure 19. Body and Wind Axis Diagram 39

NOMENCLATURE

a_z = normal body-axis acceleration
Cov = covariance matrix
C_{D_W} = coefficient of drag, wind axis
C_L = coefficient of lift
FTE = flight test engineer
g = gravity
IMU = inertial measurement unit
J = cost function
j = imaginary number = $\sqrt{-1}$
KIAS = indicated airspeed in knots
m = aircraft mass
M = pitch moment
q = pitch rate
$\bar{q}$ = dynamic pressure, $\frac{1}{2}\rho V_T^2$
Re( ) = real part
s = standard error
S = wing reference area
T = thrust
V = observed airspeed
UTSI = University of Tennessee Space Institute
Z = body-axis Z force
α = angle of attack
β = angle of side slip
δe = elevator deflection
Δ = change
ϕ = bank angle
θ = parameter vector, pitch angle
σ^2, *Var* = variance

superscripts

T = transpose
$\hat{}$ = estimate
$\tilde{}$ = Fourier transform
-1 = matrix inverse
$\dagger$ = complex conjugate transpose

subscripts

o = reference value or bias term

INTRODUCTION

Flight testing is an expensive endeavor, from planning to execution to data analysis. In many cases, flight testing can cost anywhere between a thousand dollars per flight test hour to tens of thousands of dollars per flight test hour. Therefore, it is imperative that high quality measurements and the necessary flight data be recorded in the most efficient manner. Flight test maneuvers to collect aircraft stability and control data include doublets, impulses, multi-steps and frequency sweeps[1]. Recently, computerized multi-sine inputs were added to a large amplitude maneuver to maximize stability and control flight testing efficiency[2]. In another work, manual piloted fuzzy inputs were performed during a large amplitude maneuver[3]. Previous stability and control flight testing on UTSI's Piper Saratoga was performed using system identification to estimate stability and control derivatives using a small amplitude maneuver and has other useful information regarding the Piper Saratoga[4].

In this work, efficient flight test maneuvers to estimate longitudinal aerodynamic forces and moments are investigated using a novel maneuver for longitudinal stability and control flight testing as originally introduced and performed in Ref. 3 and Ref. 5. Manual piloted doublet inputs were added to a longitudinal large amplitude maneuver and compared to longitudinal small amplitude manual piloted doublet inputs in flight.

In general, small amplitude manual doublets take 5 to 10 seconds to complete, but can take several minutes to setup. This setup time is required to ensure a proper trim airspeed. In contrast, a large amplitude maneuver can effectively cover a range of airspeeds in less time, increasing the efficiency and cost effectiveness of this method.

Subsequent chapters of this thesis explain the necessary theoretical background information, as well as provide a brief description of the research aircraft and the instrumentation system. Additional sections describe maneuver design and several maneuver variations that accommodate the experimental investigation through stall and recovery. The thesis closes with flight test results from UTSI's Piper Saratoga. This work was originally presented as an AIAA conference paper[6].

All dimensional modeling results were produced using an equation-error method in the frequency domain[1,7]. All aircraft modeling and data analysis in this work were completed by

modifying software written in MATLAB® for system identification, called System IDentification Programs for AirCraft, or SIDPAC. SIDPAC comes with Ref. 1, and is available to the public. The SIDPAC software was developed at NASA Langley by Dr. Eugene A. Morelli.

CHAPTER 1
THEORETICAL BACKGROUND

Desirable stability and control characteristics of aircraft are dependent on the mission and purpose of the aircraft. Fighter aircraft are designed to be maneuverable and in general, are not stable, but have good control characteristics. Transport aircraft are designed to be stable, but are not very maneuverable. Stability and control derivatives determine the un-augmented aircraft's stability and control.

Stability and control derivatives are measures of how forces and moments change with respect to airspeed, altitude, angle of attack, control surfaces deflections etc., about a defined trim flight condition. A trim flight condition is where the sum of the forces and moments on the aircraft are equal to zero. For a stable aircraft, in trimmed flight, the pilot can let go of the flight controls and the aircraft will remain in the trim condition, assuming a steady atmosphere. Aircraft equations of motion are used to investigate aircraft static and dynamic motion.

Stability and control derivatives are both measures of forces and moments on an aircraft as the flight conditions change. They differ in that stability derivatives are the effect of flight condition parameter change, such as angle of attack or pitch rate, on the forces and moments. These flight condition parameters are called states. Whereas control derivatives are the effect of control surface position change, such as elevator, ailerons and rudder deflections, on the forces and moments.

As flight conditions change, the stability and control derivatives change. To create an aircraft model structure based on flight data, samples of stability and control derivatives throughout the operational range must be collected. This chapter will begin with the derivation of the equations of motion.

1.1 Derivation of the Equations of Motion

The equations of motion for an aircraft can be written as follows in the wind axis frame. (See Fig. 19 in the appendix)

$$\dot{V} = -\frac{\bar{q}S}{m} C_{D_w} + \frac{T}{m}\cos\alpha\cos\beta + g\begin{pmatrix}\cos\phi\cos\theta\sin\alpha\cos\beta \\ +\sin\phi\cos\theta\sin\beta - \sin\theta\cos\alpha\cos\beta\end{pmatrix} \tag{1}$$

$$\begin{aligned}\dot{\alpha} = &-\frac{\bar{q}S}{mV\cos\beta} C_L + q - \tan\beta\left(p\cos\alpha + r\sin\alpha\right) - \frac{T\sin\alpha}{mV\cos\beta} \\ &+ \frac{g}{V\cos\beta}\left(\cos\phi\cos\theta\cos\alpha + \sin\theta\sin\alpha\right)\end{aligned} \tag{2}$$

Only the longitudinal motion was studied, therefore, $\beta = \phi = 0$. The equations then become

$$\dot{V} = -\frac{\bar{q}S}{m} C_{D_w} + \frac{T}{m}\cos\alpha + g\left(\cos\theta\sin\alpha - \sin\theta\cos\alpha\right) \tag{3}$$

$$\dot{\alpha} = -\frac{\bar{q}S}{mV} C_L + q - \frac{T\sin\alpha}{mV} + \frac{g}{V}\left(\cos\theta\cos\alpha + \sin\theta\sin\alpha\right) \tag{4}$$

Using the following trig identities to simplify the gravity terms

$$\begin{aligned}\sin\theta\cos\alpha &= \frac{1}{2}\left[\sin\left(\theta+\alpha\right) + \sin\left(\theta-\alpha\right)\right] \\ \cos\theta\sin\alpha &= \frac{1}{2}\left[\sin\left(\theta+\alpha\right) - \sin\left(\theta-\alpha\right)\right] \\ \cos\theta\cos\alpha &= \frac{1}{2}\left[\cos\left(\theta-\alpha\right) + \cos\left(\theta+\alpha\right)\right] \\ \sin\theta\sin\alpha &= \frac{1}{2}\left[\cos\left(\theta-\alpha\right) - \cos\left(\theta+\alpha\right)\right]\end{aligned} \tag{5}$$

Substituting equations (5) in to equations (3) and (4) yield

$$\dot{V} = -\frac{\bar{q}S}{m} C_{D_w} + \frac{T}{m}\cos\alpha + g\begin{pmatrix}\left[\frac{1}{2}\left[\sin\left(\theta+\alpha\right) - \sin\left(\theta-\alpha\right)\right]\right] \\ -\left[\frac{1}{2}\left[\sin\left(\theta+\alpha\right) + \sin\left(\theta-\alpha\right)\right]\right]\end{pmatrix} \tag{6}$$

$$\dot{\alpha} = -\frac{\bar{q}S}{mV}C_L + q - \frac{T\sin\alpha}{mV} + \frac{g}{V}\begin{pmatrix} \frac{1}{2}\left[\cos(\theta-\alpha)+\cos(\theta+\alpha)\right] \\ -\frac{1}{2}\left[\cos(\theta-\alpha)-\cos(\theta+\alpha)\right] \end{pmatrix} \tag{7}$$

Canceling and combining terms

$$\dot{V} = -\frac{\bar{q}S}{m}C_{D_w} + \frac{T}{m}\cos\alpha + g\left[\sin(\theta-\alpha)\right] \tag{8}$$

$$\dot{\alpha} = -\frac{\bar{q}S}{mV}C_L + q - \frac{T\sin\alpha}{mV} + \frac{g}{V}\left[\cos(\theta-\alpha)\right] \tag{9}$$

The flight-path angle equation is

$$\gamma = \theta - \alpha \tag{10}$$

Simplifying further, insert equation (10) into equations (8) and (9)

$$\dot{V} = -\frac{\bar{q}S}{m}C_{D_w} + \frac{T}{m}\cos\alpha + g\sin\gamma \tag{11}$$

$$\dot{\alpha} = -\frac{\bar{q}S}{mV}C_L + q - \frac{T\sin\alpha}{mV} + \frac{g}{V}\cos\gamma \tag{12}$$

Here the $\dot{q}$ equation is brought in from equation (97) in the appendix to do the linearizing along with the equations above. This is again assuming longitudinal motion only and therefore, $p = r = 0$ and equation (97) reduces to

$$\dot{q} = \frac{\bar{q}S\bar{c}}{I_{yy}}C_m \tag{13}$$

Linearizing the nonlinear equations of motion can be done by applying small-perturbation theory. This is executed by assuming, the test point condition to be steady, with no sideslip and wings level.

$$
\begin{array}{llll}
V = V_o + \Delta V & \dot{V} = \dot{V}_o + \Delta \dot{V} & T = T_o + \Delta T & \alpha = \alpha_o + \Delta\alpha \\
q = q_o + \Delta q & \dot{q} = \dot{q}_o + \Delta \dot{q} & \bar{q} = \bar{q}_o + \Delta \bar{q} & \gamma = \gamma_o + \Delta\gamma \\
C_{D_w} = C_{D_{w_o}} + \Delta C_{D_w} & C_L = C_{L_o} + \Delta C_L & C_m = C_{m_o} + \Delta C_m &
\end{array} \tag{14}
$$

The variables beginning with Δ are small perturbations. The airspeed and the dynamic pressure are simplified by assuming that $V \approx V_o$ and $\bar{q} \approx \bar{q}_o$. This is the case for an aircraft where $V_o >> \Delta V$.

$$
V_o + \Delta\dot{V} = -\frac{\bar{q}S}{m}\left(C_{D_o} + \Delta C_D\right) + \frac{\left(T_o + \Delta T\right)}{m}\cos\left(\alpha_o + \Delta\alpha\right) + g\sin\left(\gamma_o + \Delta\gamma\right) \tag{15}
$$

$$
\begin{aligned}
\dot{\alpha}_o + \Delta\dot{\alpha} = &-\frac{\bar{q}S}{m\left(V_o + \Delta V\right)}\left(C_{L_o} + \Delta C_L\right) + \left(q_o + \Delta q\right) \\
&-\frac{\left(T_o + \Delta T\right)\sin\left(\alpha_o + \Delta\alpha\ \right)}{m\left(V_o + \Delta V\right)} + \frac{g}{\left(V_o + \Delta V\right)}\cos\left(\gamma_o + \Delta\gamma\right)
\end{aligned} \tag{16}
$$

$$
\dot{q}_o + \Delta\dot{q} = \frac{\left(C_{m_o} + \Delta C_m\right)}{I_{yy}} \tag{17}
$$

Taking equations (11) - (13) and setting the values at the steady condition

$$
\dot{V}_o = -\frac{\bar{q}_o S}{m}C_{D_o} + \frac{T_o}{m}\cos\alpha_o + g\sin\gamma_o \tag{18}
$$

$$
\dot{\alpha}_o = -\frac{q_o S}{mV_o}C_L + q - \frac{T_o\sin\alpha_o}{mV_o} + \frac{g}{V_o}\cos\gamma_o \tag{19}
$$

$$
\dot{q}_o = \frac{\bar{q}S\bar{c}}{I_{yy}}C_{m_o} \tag{20}
$$

Subtracting the steady state condition (equations (18)-(20)) from equation (15)-(17) and inserting the ΔC_D and ΔC_L expansion gives

$$\Delta\dot{V} = -\frac{\bar{q}_o S}{m}\left(C_{D_V}\frac{\Delta V}{V_o} + C_{D_\alpha}\Delta\alpha + C_{D_q}\frac{q\bar{c}}{2V_o} + C_{D_\delta}\Delta\delta \right) - g\cos\gamma_o\left(\Delta\theta - \Delta\alpha\right) - \frac{T_o \sin\alpha_o}{m}\Delta\alpha \quad (21)$$

$$\begin{aligned}\Delta\dot{\alpha} = &-\frac{\bar{q}_o S}{mV_o}\left(C_{L_V}\frac{\Delta V}{V_o} + C_{L_\alpha}\Delta\alpha + C_{L_{\dot\alpha}}\frac{\dot\alpha\bar{c}}{2V_o} + C_{Lq}\frac{q\bar{c}}{2V_o} + C_{L_\delta}\Delta\delta \right) + q \\ &- \frac{g\sin\gamma_0}{V_o}\left(\Delta\theta - \Delta\alpha\right) - \frac{T_o\cos\alpha_o}{mV_o}\Delta\alpha\end{aligned} \quad (22)$$

$$\Delta\dot{q} = \frac{\bar{q}S\bar{c}}{I_{yy}}\left(C_{m_V}\frac{\Delta V}{V_o} + C_{m_\alpha}\Delta\alpha + C_{m_{\dot\alpha}}\frac{\dot\alpha\bar{c}}{2V_o} + C_{m_q}\frac{q\bar{c}}{2V_o} + C_{m_\delta}\Delta\delta \right) \quad (23)$$

Where δ, in this case is elevator deflection. Further simplification of these linearized equations is accomplished by using short period approximations which can accurately describes the short period response of the aircraft. The short period approximation is found by assuming $\Delta V = 0$, as during a doublet there is no change in airspeed. Therefore the equation (21) is omitted.

$$\dot{\alpha} = -\frac{\bar{q}_o S}{mV_o}\left(C_{L_\alpha}\Delta\alpha + C_{Lq}\frac{q\bar{c}}{2V_o} + C_{L_\delta}\Delta\delta \right) + q \quad (24)$$

$$\dot{q} = \frac{\bar{q}S\bar{c}}{I_{yy}}\left(C_{m_\alpha}\Delta\alpha + C_{m_{\dot\alpha}}\frac{\dot\alpha\bar{c}}{2V_o} + C_{m_q}\frac{q\bar{c}}{2V_o} + C_{m_\delta}\Delta\delta \right) \quad (25)$$

In equation (24), $\dot{\alpha}$ is a linear combination of $\Delta\dot{\alpha}$, q and $\Delta\delta$. Substitute equation (24) into (25)

$$\dot{q} = \frac{\bar{q}S\bar{c}}{I_{yy}}\left\{ C_{m_\alpha}\Delta\alpha + C_{m_{\dot\alpha}}\frac{\bar{c}}{2V_o}\left[q - \frac{\bar{q}_o S}{mV_o}\left(C_{L_\alpha}\Delta\alpha + C_{Lq}\frac{q\bar{c}}{2V_o} + C_{L_\delta}\Delta\delta \right) \right] + C_{m_q}\frac{q\bar{c}}{2V_o} + C_{m_\delta}\Delta\delta \right\} \quad (26)$$

Distributing and using the dynamic pressure as $\bar{q}_o = 1/2\rho V_o^2$, and using the following definitions,

$$\text{for the } \Delta\alpha \text{ terms } \Rightarrow \; C'_{m_\alpha} = C_{m_\alpha} - \frac{\rho S\bar{c}}{4m} C_{m_{\dot{\alpha}}} C_{L_\alpha} \tag{27}$$

$$\text{for the } \frac{q\bar{c}}{2V_o} \text{ terms } \Rightarrow \; C'_{m_q} = C_{m_q} + C_{m_{\dot{\alpha}}} \left(1 - \frac{\rho S\bar{c}}{4m} C_{L_q} \right) \tag{28}$$

$$\text{for the } \Delta\delta \text{ terms } \Rightarrow \; C'_{m_\delta} = C_{m_\delta} - \frac{\rho S\bar{c}}{4m} C_{m_{\dot{\alpha}}} C_{L_\delta} \tag{29}$$

gives the following equation.

$$\dot{q} = \frac{\bar{q}S\bar{c}}{I_{yy}} \left(C'_{m_\alpha} \Delta\alpha + C'_{m_q} \frac{q\bar{c}}{2V_o} + C'_{m_\delta} \Delta\delta \right) \tag{30}$$

Other force equations can be developed from the accelerometer outputs. For longitudinal motion only,

$$a_x = \frac{1}{m} \left(\bar{q}SC_x + T \right) \tag{31}$$

$$a_z = \frac{1}{m} \left(\bar{q}SC_Z \right) \tag{32}$$

For steady level, un-accelerated flight the a_x equation is dropped. Linearizing the a_z equation with $\Delta V = 0$,

$$\Delta a_z = \frac{\bar{q}_o S}{m} \Delta C_Z \tag{33}$$

By definition, from translation the perturbations of ΔC_Z is[1],

$$\Delta C_Z = \left(C_{L_o} \sin\alpha_o - C_{D_o} \cos\alpha_o \right) \Delta\alpha - \cos\alpha_o \Delta C_L - \sin\alpha_o \Delta C_D \tag{34}$$

Dropping the ΔC_D term, as it is assumed there is no change in drag, and substituting equation (34) into equation (33) provides the linearized equation for the vertical acceleration for the short period approximation.

$$\Delta a_z = \frac{\bar{q}_o S}{m}\left[\left(C_{L_o}\sin\alpha_o - C_{D_o}\cos\alpha_o\right)\Delta\alpha - \cos\alpha_o \Delta C_L\right] \tag{35}$$

Substituting the ΔC_L expression into equation (35),

$$\Delta a_z = \frac{\bar{q}_o S}{m}\left[\left(C_{L_o}\sin\alpha_o - C_{D_o}\cos\alpha_o\right)\Delta\alpha - \cos\alpha_o\left(C_{L_\alpha}\Delta\alpha + C_{Lq}\frac{q\bar{c}}{2V_o} + C_{L_\delta}\Delta\delta\right)\right] \tag{36}$$

At low trim angles of attack α_o, the $\Delta\alpha$ term is small and $\cos\alpha_o \approx 1$, such that,

$$\Delta a_z \approx -\frac{\bar{q}_o S}{m}\left(C_{L_\alpha}\Delta\alpha + C_{Lq}\frac{q\bar{c}}{2V_o} + C_{L_\delta}\Delta\delta\right) \tag{37}$$

The three linear equations, equations (24), (30) and (37), are for the short period approximation and are restated.

$$\dot{\alpha} = q - \frac{\bar{q}_o S}{mV_o}\left(C_{L_\alpha}\Delta\alpha + C_{Lq}\frac{q\bar{c}}{2V_o} + C_{L_\delta}\Delta\delta\right) \tag{38}$$

$$\dot{q} = \frac{\bar{q}S\bar{c}}{I_{yy}}\left(C'_{m_\alpha}\Delta\alpha + C'_{m_q}\frac{q\bar{c}}{2V_o} + C'_{m_\delta}\Delta\delta\right) \tag{39}$$

$$\Delta a_z = -\frac{\bar{q}_o S}{m}\left(C_{L_\alpha}\Delta\alpha + C_{Lq}\frac{q\bar{c}}{2V_o} + C_{L_\delta}\Delta\delta\right) \tag{40}$$

The equations above show the stability and control derivatives in their non-dimensional form, they can also be written in dimensional form.

$$L_\alpha = \frac{\bar{q}_o S}{mV_o}C_{L_\alpha} \qquad L_q = \frac{\bar{q}_o S\bar{c}}{2mV_o^2}C_{L_q} \qquad L_\delta = \frac{\bar{q}_o S}{mV_o}C_{L_\delta} \tag{41}$$

$$M_\alpha = \frac{\bar{q}_o S\bar{c}}{I_{yy}}C'_{m_\alpha} \qquad M_q = \frac{\bar{q}_o S\bar{c}^2}{2V_o I_{yy}}C'_{m_q} \qquad M_\delta = \frac{\bar{q}_o S\bar{c}}{I_{yy}}C'_{m_\delta} \tag{42}$$

Making the three linear equations in terms of dimensional derivatives from equations (41) and (42) where $q = \Delta q$.

$$\dot{\alpha} = -L_\alpha \Delta\alpha + \left(1 + L_q\right) q - L_\delta \Delta\delta \tag{43}$$

$$\dot{q} = M_\alpha \Delta\alpha + M_q q + M_\delta \Delta\delta \tag{44}$$

$$\Delta a_z = -\frac{V_o}{g}\left(L_\alpha \Delta\alpha + L_q q + L_\delta \Delta\delta\right) \tag{45}$$

At low angles of attack it can be stated, $-L = Z\cos\alpha \approx Z$, the dimensional stability and control derivatives then become,

$$Z_\alpha = \frac{\bar{q}_o S}{m V_o} C_{Z_\alpha} \qquad Z_q = \frac{\bar{q}_o S \bar{c}}{2 m V_o^2} C_{Z_q} \qquad Z_\delta = \frac{\bar{q}_o S}{m V_o} C_{Z_\delta} \tag{46}$$

$$M_\alpha = \frac{\bar{q}_o S \bar{c}}{I_{yy}} C'_{m_\alpha} \qquad M_q = \frac{\bar{q}_o S \bar{c}^2}{2 V_o I_{yy}} C'_{m_q} \qquad M_\delta = \frac{\bar{q}_o S \bar{c}}{I_{yy}} C'_{m_\delta} \tag{47}$$

The three dimensional linear equations then become,

$$\dot{\alpha} = Z_\alpha \Delta\alpha + \left(1 + Z_q\right) q + Z_\delta \Delta\delta \tag{48}$$

$$\dot{q} = M_\alpha \Delta\alpha + M_q q + M_\delta \Delta\delta \tag{49}$$

$$\Delta a_z = -\frac{V_o}{g}\left(Z_\alpha \Delta\alpha + Z_q q + Z_\delta \Delta\delta\right) \tag{50}$$

There are two force equations and one moment equation. Only one equation for the force is needed. The *Z* body axis acceleration, a_z, does not include an inertial term. Also, the a_z measurement is directly applicable to estimating the dimensional derivatives associated with *Z*. Whereas using the dynamic equation for α involves the extra approximation, $-L = Z\cos\alpha \approx Z$. Thus, the equations for a_z yields better estimates results for the aerodynamic parameters related with the *Z* force in the body axis.

$$\dot{q} = M_\alpha \Delta\alpha + M_q q + M_\delta \Delta\delta \tag{51}$$

$$\Delta a_z = -\frac{V_o}{g}\left(Z_\alpha \Delta\alpha + Z_q q + Z_\delta \Delta\delta\right) \tag{52}$$

Rearranging and dropping the Δ prefix the equations become

$$\dot{q} = M_{\alpha}\alpha + M_{q}q + M_{\delta e}\delta e \tag{53}$$

$$-\frac{g}{V}a_{z} = Z_{\alpha}\alpha + Z_{q}q + Z_{\delta e}\delta e \tag{54}$$

Equations (53) and (54) are the moment and force equations, respectively, used to calculate the dimensional force and moment stability and control derivatives.

1.2 System Identification

System identification is used to determine the aircraft stability and control derivatives from the aircraft equations of motion. System identification determines the mathematical model of a physical system given the inputs of the system, outputs of the system, and the form of the mathematical model of the system. Two different methods of parameter identification are typically used, the output-error method and the equation-error method. The output error method is an iterative procedure where all the measurements and parameters corrections are computed simultaneously[1]. The equation-error method is based on ordinary least-squares regression, where the aerodynamic stability and control derivatives are estimated by minimizing the error between measured and modeled aerodynamic forces and moments[1]. Additionally, the equation-error method does not need to integrate the equations of motion to get model output because the matching is done in the equations of motion themselves. This makes the equation-error method useful when identifying nonlinear models, where several aerodynamic models may be evaluated.

System identification can be performed in the time domain or in the frequency domain. The frequency domain is advantageous because converting the signals using the chirp-z transform can filter out the noise in the signals[1]. Likewise there is no need for tedious calibration of raw signal values because only the dynamic content of the data is considered. For this work, the equation-error method of system identification was performed in the frequency domain.

The equation-error method in the frequency domain is used to calculate the aerodynamic parameter estimates that minimize the sum of the squared differences between values of the

dimensional stability and control derivatives determined from measured flight data and corresponding model values. The dimensional model values for the forces and moments are computed by substituting measured states and controls and known values into the linear equations (53) and (54) and the following nonlinear model structure equations.

$$\dot{q} = M_{\alpha^2}\alpha^2 + M_{\alpha}\alpha + M_q q + M_{\delta e}\delta e \tag{55}$$

$$-\frac{g}{V}a_z = Z_{\alpha^2}\alpha^2 + Z_{\alpha}\alpha + Z_q q + Z_{\delta e}\delta e \tag{56}$$

Equations (53) and (54) represent a linear state space model, which is used for small amplitude maneuver and equations (55) and (56) represent a nonlinear state space model, which is used for the large amplitude maneuvers. The maneuvers and determination of the nonlinear equations are discussed in chapters 3 and 4 respectively. Least squares regression in the frequency domain is used to solve for the force and moment estimates by using equations (53)-(56).

1.3 Converting Measured Data to the Frequency Domain

Since all the flight test data was measured in the time domain it needs to be converted into the frequency domain. Conversion from the time domain to the frequency domain is based on the Fourier integral equation. For a finite function the equation is

$$\tilde{X}(f) \equiv \int_0^T x(t)e^{-j\omega t}\mathrm{d}t \tag{57}$$

$x(t)$ is the time domain data and $\tilde{x}(f)$ is the converted data in the frequency domain. The cyclic frequency, *f*, can also be described in terms of angular frequency, $\omega = 2\pi f$. The finite Fourier transform can be approximated when the time function $x(t)$ is sampled at discrete, evenly spaced time intervals of Δt.

$$\tilde{X}(f) \approx \Delta t \sum_{i=0}^{N-1} x(i)e^{-j(2\pi fi)\Delta t} \tag{58}$$

where

$$\Delta t = \frac{T}{(N-1)} \qquad t_i = i\,\Delta t \qquad x(i) \equiv x(t_i) = x(i\,\Delta t) \qquad i = 0,1,2,...,N-1 \tag{59}$$

The time index, *i*, starts at 0, and the total number of data points in the time domain is *N*.

Instead of looking at the discrete Fourier transform over the entire range of frequencies, as in Eq (58), the discrete Fourier transform can focus on a specific frequencies of interest. The approximation of the finite Fourier transform in equation (58) can be described by separate frequency bins in which the signal is being divided. The frequencies are chosen as

$$f_k = \frac{k}{N\Delta t} \quad \text{or} \quad \omega_k = 2\pi f_k = 2\pi \frac{k}{N\Delta t} \qquad k = 0,1,2,...,N-1 \tag{60}$$

By using the frequencies of interest, f_k, in equation (60), the approximation of the finite Fourier transform in equation (58) becomes

$$\tilde{X}(k) \approx \Delta t \sum_{i=0}^{N-1} x(i) e^{-j(2\pi k/N)i} \qquad k = 0,1,2,...,N-1 \tag{61}$$

It is sufficient to compute the finite Fourier transform for only the first *M* frequencies of interest as was defined in equation (60), where

$$M = \begin{cases} N/2+1 & \text{for } N \text{ even} \\ (N+1)/2 & \text{for } N \text{ odd} \end{cases} \tag{62}$$

The discrete frequencies f_k are shown to be dependent upon the number of samples and time period. This leads to values of *M* that represent the limitation of the discrete Fourier

transform, specifically the frequencies contained in a sampled time history must be below the Nyquist frequency which is defined as one half the sampling rate.

To apply the chirp-z transform, select M discrete frequencies in the frequency band [$f_0 \ldots f_1$], such that

$$f_k = f_0 + k\Delta f \qquad k = 0,1,2,\ldots,M-1 \tag{63}$$

The arbitrarily selected frequency resolution can be determined by

$$\Delta f = \left(\frac{f_1 - f_0}{M} \right) \tag{64}$$

Equation (61) then can be written as

$$\tilde{X}_k \equiv \sum_{i=0}^{N-1} x_i e^{-j(2\pi f_k)t_i} = \sum_{i=0}^{N-1} x_i e^{-j(2\pi f_0)i\Delta t} e^{-j(2\pi k\Delta f)i\Delta t} \qquad k = 0,1,2,\ldots,M-1 \tag{65}$$

Simplifying the previous equation by defining ϕ, $\Delta\phi$, A, and Z

$$\begin{aligned} \varphi &= 2\pi f_0 \Delta t & \Delta\varphi &= 2\pi\Delta f\,\Delta t \\ A &= e^{j\varphi_0} & Z &= e^{j\Delta\varphi} \end{aligned} \tag{66}$$

Joining equations (65) and (66) the following equation represents the discrete Fourier transform with an arbitrary frequency band and resolution known as the chirp-z transform.

$$\tilde{X}_k \equiv \sum_{i=0}^{N-1} x_i A^{-i} Z^{ki} = \sum_{i=0}^{N-1} x_i \left[AZ^k \right]^{-i} \tag{67}$$

As k increases, the quantity AZ^k represents a contour along the unit circle in the z plane. (see figure 18 in the appendix) The quantity ϕ_0 is the angular location on the unit circle associated with the starting frequency f_0, and $\Delta\phi$ represents the incremental angular step along the unit circle in the z plane for each frequency increment Δf, corresponding to each increment in k [8,9].

1.4 Estimating the Dimensional Stability and Control Derivatives using Equation-Error

Substituting measured states and controls for each of the equations (53)-(56) results in an over-determined set of equations for the unknown aerodynamic parameters. This over-determined problem can be solved by using a standard least-squares method in the frequency domain[1].

$$\tilde{z} = \tilde{X}\theta + \tilde{v} \tag{68}$$

where,

$$\tilde{z} = \begin{bmatrix} j\omega_1 \tilde{q}_n(\omega_1) \\ \vdots \\ j\omega_m \tilde{q}_n(\omega_m) \end{bmatrix} \qquad \tilde{X} = \begin{bmatrix} \tilde{\alpha}(\omega_1) & \tilde{q}(\omega_1) & \tilde{\delta e}(\omega_1) \\ \vdots & \vdots & \vdots \\ \tilde{\alpha}(\omega_m) & \tilde{q}(\omega_m) & \tilde{\delta e}(\omega_m) \end{bmatrix} \tag{69}$$

The matrix $\tilde{X}$ is created by using measured data, with each column representing an independent variable that is being used for the regression, i.e. a regressor.

$$\theta = \begin{bmatrix} M_\alpha & M_q & M_{\delta e} \end{bmatrix} \tag{70}$$

$$\tilde{v} = \begin{bmatrix} \tilde{v}(\omega_1) \cdots \tilde{v}(\omega_m) \end{bmatrix}^{\mathrm{T}} \tag{71}$$

$$J(\theta) = \tfrac{1}{2}\left(\tilde{z} - \tilde{X}\theta\right)^{\dagger}\left(\tilde{z} - \tilde{X}\theta\right) \tag{72}$$

For least-squares, the best estimator of θ comes from minimizing the sum of squared differences between the dependent variable measurements, $\tilde{z}$, and the model. The least-squares solution for the unknown parameter vector θ is[1]

$$\hat{\theta} = \left[\mathrm{Re}\left(\tilde{X}^{\dagger}\tilde{X}\right)\right]^{-1} \mathrm{Re}\left(\tilde{X}^{\dagger}\tilde{z}\right) \tag{73}$$

The estimated parameter covariance matrix is computed from[1]

$$Cov\left(\hat{\theta}\right) = \hat{\sigma}^2 \left[\mathrm{Re}\left(\tilde{X}^{\dagger} \tilde{X} \right) \right]^{-1} = \left[C_{ij} \right] \quad i, j = 1, 2, ..., n_p \tag{74}$$

$$\hat{\sigma}^2 = \frac{\left(z - \hat{y}\right)^{\dagger} \left(z - \hat{y}\right)}{\left(m - n_p\right)} \qquad \hat{y} = X\hat{\theta} \tag{75}$$

The standard errors of the estimated parameters are given by the square root of the diagonal elements of the matrix.

$$s\left(\hat{\theta}_j\right) = \sqrt{C_{jj}} \quad j = 1, 2, ..., n_p \tag{76}$$

To apply equation-error parameter estimation in the frequency domain, the data must be transformed using a high-accuracy chirp-z Fourier transform as in equation (67). It allows the use of arbitrary frequencies and resolutions for the transformation[1,8]. For the present work, the frequencies used for all high-accuracy chirp-z Fourier transformations were

$$f = \left[\begin{array}{cccccc} 0.10 & 0.14 & \ldots & 1.94 & 2.0 \end{array} \right]^T \ \mathrm{Hz} \tag{77}$$

Frequency resolution of 0.04 Hz generally works well[1]. The lower bound was chosen as 0.1 Hz and the upper bound should be chosen to include the dynamics of interest, for the Piper Saratoga it is around 2.0 Hz. The frequency band acts as a filter, passing all frequencies below 2.0 Hz and rejecting frequencies above 2.0 Hz, which effectively eliminates modeling error due to structural flexing and other high frequency effects. Likewise, frequencies below 0.1 Hz are excluded, which removes trim values and measurement biases.

In the frequency domain, the noise variance magnitude is not constant over all frequencies[7]. However, if the frequency analysis is limited to the rigid-body dynamics, then the residuals are approximately constant. In this case, the estimated parameter error bars can be calculated without corrections using equations (74)-(76).

CHAPTER 2
RESEARCH AIRCRAFT

2.1 Aircraft

The UTSI Piper Saratoga, PA 32-301, tail number N22UT, has fixed landing gear and a maximum take-off weight of 3600 lbs. It has the seating capacity to carry two pilots and four FTEs. The Piper Saratoga is a single engine aircraft that is equipped with a 300 HP Lycoming IO-540-K1G5 engine attached to a Hartzell constant speed three bladed propeller. The aircraft has an approximate clean stall speed of 62 KIAS, and a full flap stall speed of 58 KIAS at sea level. The maximum velocity of the aircraft is restricted to 150 KIAS due to structural limits imposed by the research air data boom that is mounted on the right wingtip.



Figure 1. Piper Saratoga, PA 32-301

2.2 Instrumentation

The research aircraft has two air data systems: the production system and the research system. The research air data system is independent of the production air data system. The pressure sensing gauges for the pilot are governed by the factory pitot-static mast under the left wing as shown in Fig. 2. The factory system has a total pressure port, static pressure port, and a drain port. The Piper Saratoga is also equipped with a research air data system installed under the right wing as shown in Fig. 3. It consists of a total temperature probe, Kiel probe, total pressure port, and a static pressure probe. The third pressure sensing system is a pair of additional static ports located on the aft fuselage as shown in Fig. 4. Also, an IMU is installed on the aircraft, as well as

load cells and potentiometers to record control surface deflections and forces. The Piper Saratoga also has a wingtip boom that contains flow angle vanes for angle of attack and angle of side slip as shown in Fig. 5. A data acquisition system (DAS) capable of recording data at 20 Hz is used to record the flight data measured from the instrumentation.



Figure 2. Factory Installed ADS



Figure 3. Flight Test ADS



Figure 4. After Market Static Ports



Figure 5. Air Data Vanes

CHAPTER 3
MANERVER DESIGN

To achieve longitudinal stability and control estimates for forces and moments, the short period mode needs to be excited in order to produce independent regressor signals. The short period motion is a rapid pitching motion about the center of gravity. The period is short enough that the speed is relatively constant and the oscillations are essentially an angle of attack and pitch rate variation. Also, the short period has a period of a few seconds and is usually heavily damped.

To find the short period of the aircraft, several different maneuvers were tested. Initially, several doublets with varying frequency and amplitude were performed to discover which variation gave the best results. Other inputs were also performed, such as 2-1-1 and 3-2-1-1. Performing two doublets, as well as three doublets, back to back was also tested. Two doublets, or a multiple doublet, back to back produced the best regressor signals for analysis as they were unique and usually had smaller percentage error than a normal doublet.

3.1 Maneuver Implementation

To implement the maneuvers, audio tones were used to cue the pilot. A multi-output tone generator was developed to output tones in a variety of sequences. Figure 6 shows the front panel of a LabVIEW® virtual instrument with the optional pilot input cues. The red dots indicate where the tones are played. The 1-1 sequence was played twice back to back for the pilot to execute the multiple doublet maneuvers.

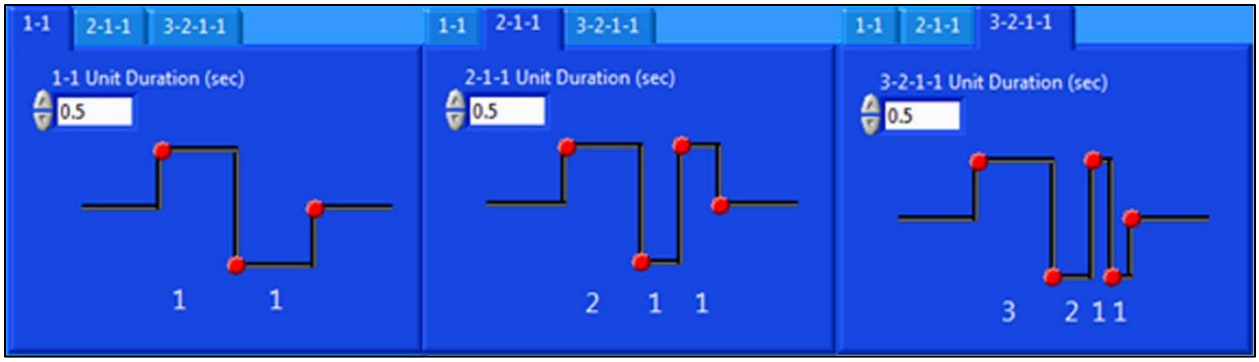


Figure 6. LabVIEW® Virtual Instrument Input Tones

Figure 7 depicts the process from the FTE command to the elevator control surface deflection.

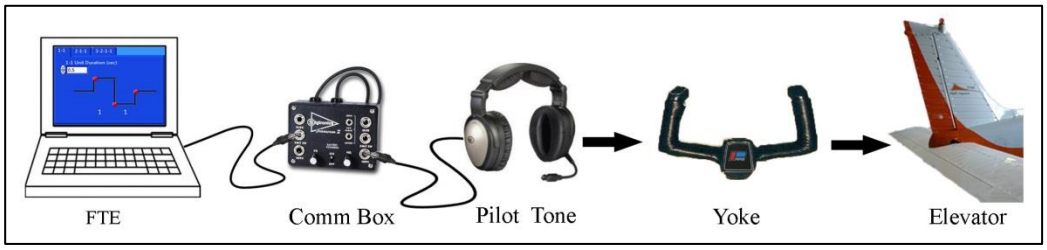


Figure 7. Input Tones Implementation

3.2 Small Amplitude Maneuvers for Local Aerodynamic Modeling

Several small amplitude maneuvers were performed for the local aerodynamic modeling throughout the normal operating range of the aircraft. The small amplitude maneuvers were implemented in increments of 10 KIAS from 80 to 120 KIAS. The aircraft was trimmed in a straight and level flight condition and multiple doublets were performed at each airspeed. In this thesis, the small amplitude maneuver estimates are used as truth values for comparison with the large amplitude maneuver estimates.

3.3 Large Amplitude Maneuvers for Global Aerodynamic Modeling

The large amplitude maneuver for the global aerodynamic model is performed by the pilot flying doublets on top of a steady pull up to stall and push over in increments of 10 KIAS. This

large amplitude maneuver was performed using two different techniques. The first technique applied small amplitude stick doublets up to 80 KIAS as can be observed in Fig 11. The second technique applied small amplitude stick doublets through stall and continued the doublets in the push over back to the trim velocity as can be observed in Fig. 16.

CHAPTER 4
FLIGHT TEST RESULTS

4.1 Longitudinal Small Amplitude Maneuvers Results

Small Amplitude maneuvers were performed at 80, 90, 100, 110, and 120 KIAS. Figure 8 is an example of the time series plots recorded from a multiple doublet input at 100 KIAS. All tested airspeeds resulted in similar plots, but are not shown. Table 1, located in the appendix, has a summary of the small amplitude maneuver results from 80 to 120 KIAS airspeed range in 10 knot increments. In almost all cases, the estimates have less than 10 percent error which shows that the input excited the short period, and therefore the regressor signals were unique. The exceptions are in the Z_q and $Z_{\delta e}$ estimates at 90 and 120 KIAS. This is most likely due to the difficulty in estimating these Z force derivatives at low angles of attack.

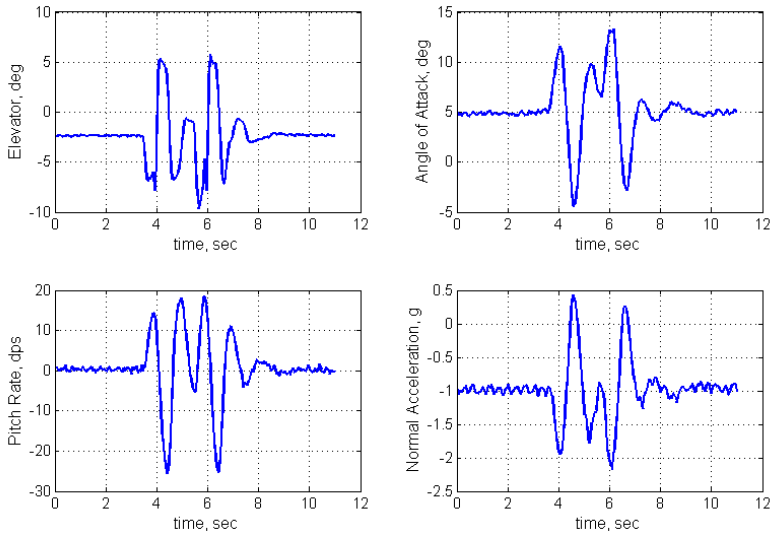


Figure 8. Measured Time Series – Multiple Doublets at 100 KIAS

Figure 9 shows a sample of the equation-error modeling results for the body-axis Z force in the frequency domain. As shown in Fig. 9 the *Z* force short period frequency is seen to be at 1 Hz. The peaks at the low and high frequencies are where other frequencies were excited during this particular maneuver.

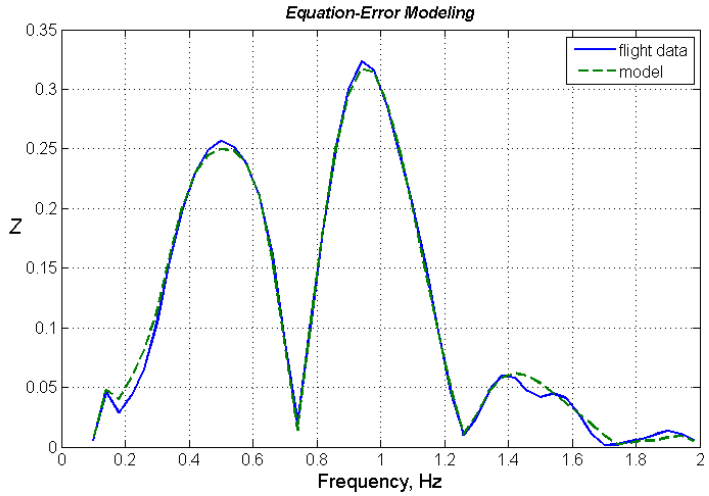


Figure 9. Body-Axis Z Force vs. Frequency – Multiple Doublets at 100 KIAS

Figure 10 shows a sample of the equation-error modeling results for the pitching moment in the frequency domain. The model matches the flight data well with the exception at the lower and higher frequencies where the flight data is seen to deviate from the model.

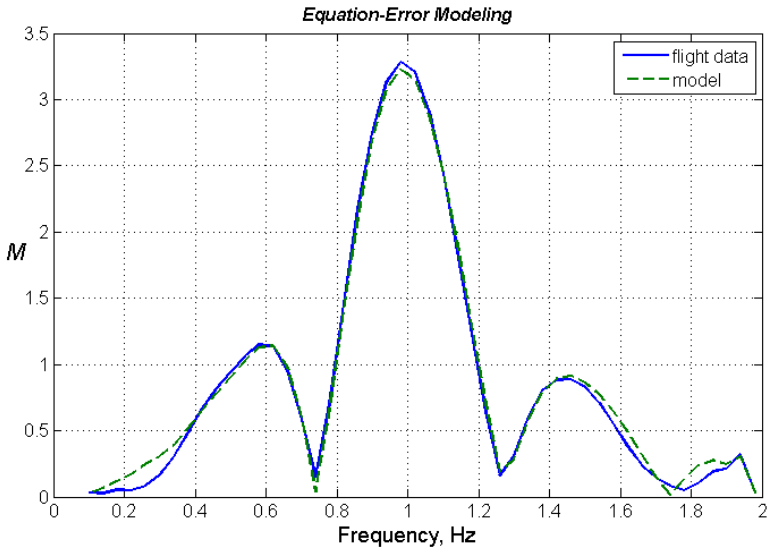


Figure 10. Pitch Moment M vs. Frequency – Multiple Doublets at 100 KIAS

4.2 Large Amplitude Maneuver Results

The large amplitude maneuver time series depicted in Fig. 11 represents a longitudinal only large amplitude maneuver. The maneuver consists of a steady pull-up from trimmed straight and level flight with longitudinal doublets at 10 knot increments from 120 to 80 knots, where the 80 knot lower bound is near the edge of stall. Duration of the total maneuver was less than 40 seconds and 5 doublets were performed during the maneuver at 5 different airspeeds. Figures 12 and 13 are measured and modeled body-axis *Z* force and pitching moment *M* verses frequency for this maneuver.

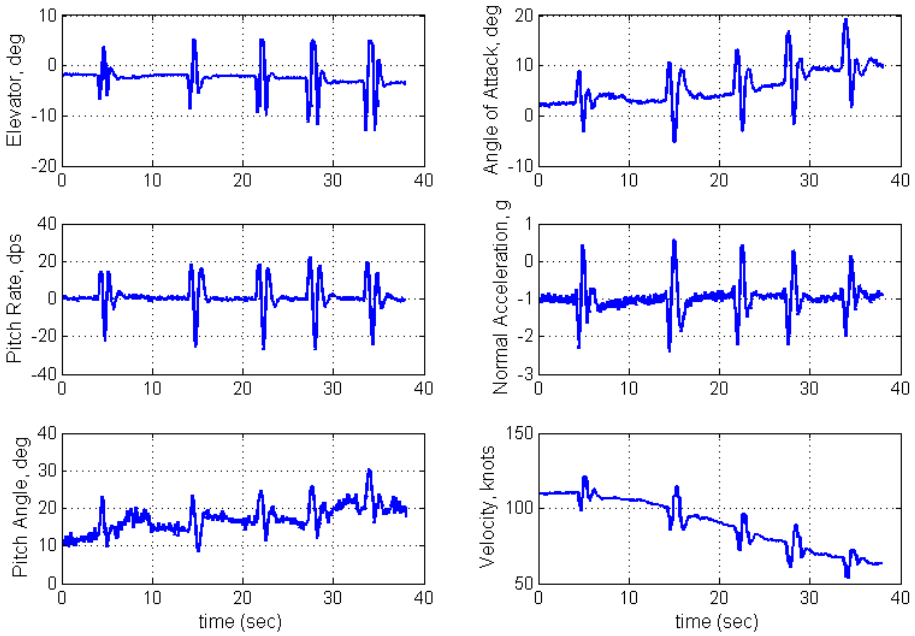


Figure 11. Measured Time Series – Longitudinal Large Amplitude Maneuver without Stall

Figure 12 shows a sample of the equation-error modeling frequency for the body axis force for the large amplitude maneuver. As shown in Fig. 12 the short period frequency is around 1 Hz. While figures 12 and 13 do not appear to match as well as in the Figs. 9 and 10, yet still produce errors as small as 6 percent.

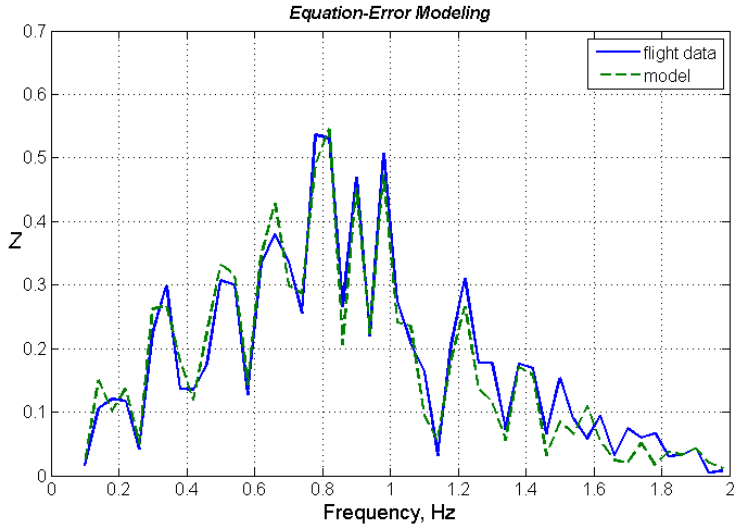


Figure 12. Longitudinal Large Amplitude Maneuver Z vs. Frequency

Figure 13 shows a sample of the equation-error modeling frequency for the pitch moment for the large amplitude maneuver. As shown in Fig. 13, the short period frequency appears to be around 1 Hz.

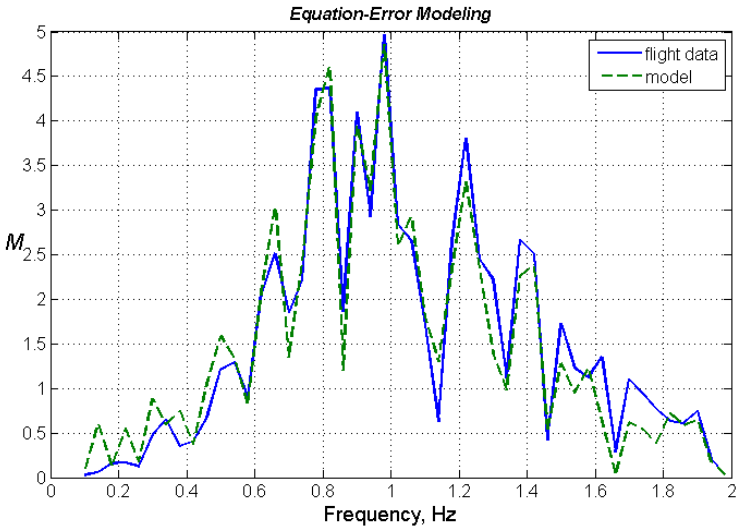


Figure 13. Longitudinal Large Amplitude Maneuver M vs. Frequency

The Piper Saratoga has a NACA 66_2-415 airfoil, the lift curve slope of the airfoil is shown in Fig. 14 for representative cruise Reynolds numbers. The aerodynamics are assumed to be

represented by a nonlinear model due to flow separation at high angles of attack. The question then becomes which regressors are nonlinear.

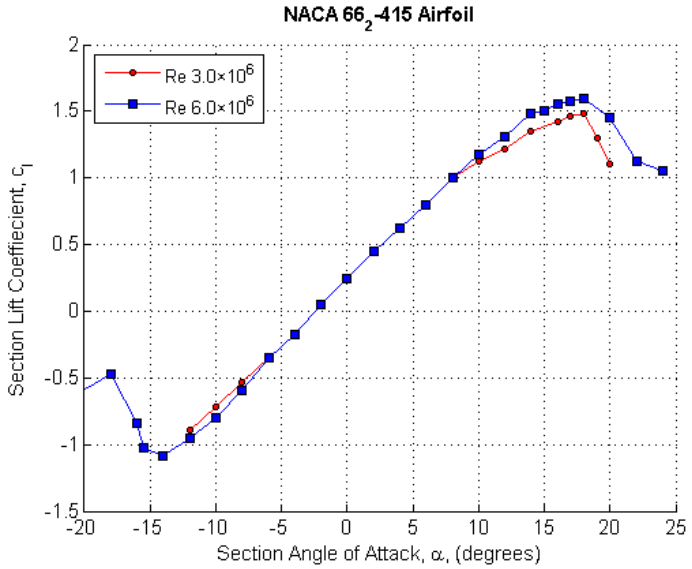


Figure 14. NACA 66$_2$-415 Airfoil Lift Curve Slope

The nonlinear regressors can be found by using step wise regression[1]. Step wise regression was done on the flight data results from the large amplitude maneuver that was performed through stall. The step wise regressions are shown in Table 2. Table 2 shows the parameter estimates and statistical metrics for each step in the model structure determination[1]. At the start, the partial correlations, r, of each regressor with the response variable Z are computed. As each regressor is evaluated in the model, a corresponding parameter estimate and F_0 statistic are computed. In step 1, the $Z\alpha$ term is chosen first because it has the largest correlation value. In step 2, the $Z\alpha^2$ term has the largest correlation value and is chosen next. This process is repeated for the Z and M terms. Regressors q^2 and δe^2 have a small contribution and are omitted from the model structure. Other nonlinear regressor combinations were also explored, but only the α^2 terms for both forces and moments were used for the nonlinear model.

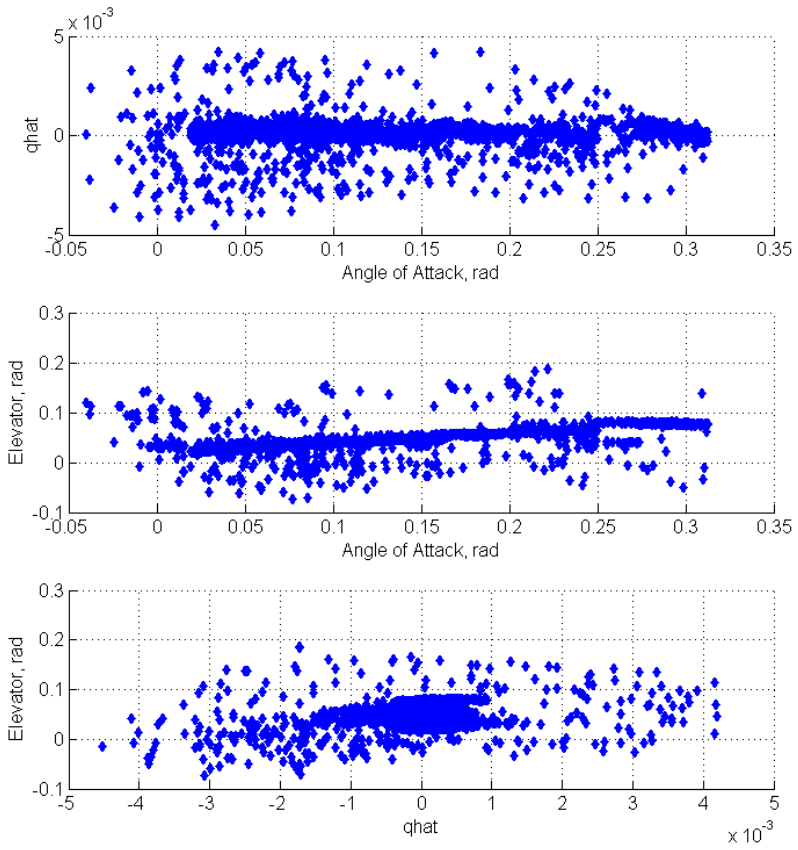


Figure 15. Longitudinal Large Amplitude Maneuver Independent Variable Cross Plots

Figure 15 shows the cross plots of angle of attack, elevator deflection, and non-dimensional pitch rate. This shows the effectiveness of the maneuver at covering the flight envelope of the aircraft. If a large portion of the cross plot area is covered then a significant amount of data was gathered from one flight test maneuver. Cross plots are also a graphical indication of pair wise correlation between independent variables[1]. The independent variables, i.e. the regressors, must show a low pair wise correlation for the parameter identification technique to work. If the cross plots were approximately a straight line, then they would be highly correlated and the results from the parameter identification technique would not be accurate.

Another longitudinal large amplitude maneuver was performed through stall and was continued from stall back the initial trim speed of 120 KIAS. Time series plots from the large amplitude maneuver are in Fig. 16. It should be noted that the stall angle of attack is around 17 degrees, which is nearly identical to the stall angle of attack in Fig. 14.

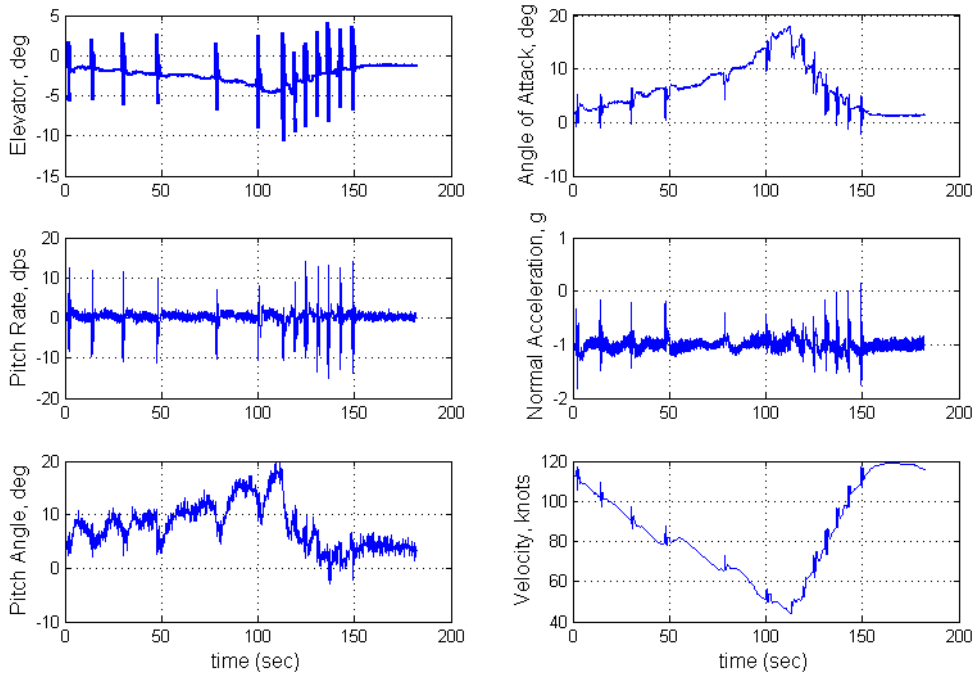


Figure 16. Measured Time Series – Longitudinal Large Amplitude Maneuver through Stall

Table 3 compares two large amplitude maneuvers, one near stall and the other through stall and recovery. The large amplitude maneuver up to stall shows a significant percentage error, whereas the large amplitude maneuver through stall and recovery resulted in improved percentage errors. Improvements were seen in all estimates except in M_q.

In order to build confidence with large amplitude maneuver estimates, small amplitude maneuver estimates were compared with data sets from the same airspeeds cut from the large amplitude maneuvers. The cut data sets were taken from the large amplitude maneuver from about a second before and about a second after each doublet performed in the maneuver. The results in Table 1 compare small amplitude maneuvers and cut data sets from the large amplitude maneuvers. The cut data sets from the large amplitude maneuvers were almost always within the confidence interval of the small amplitude maneuvers. This suggests that large amplitude maneuvers can be used to obtain similar results that would be obtained with small amplitude maneuvers, but in less time.

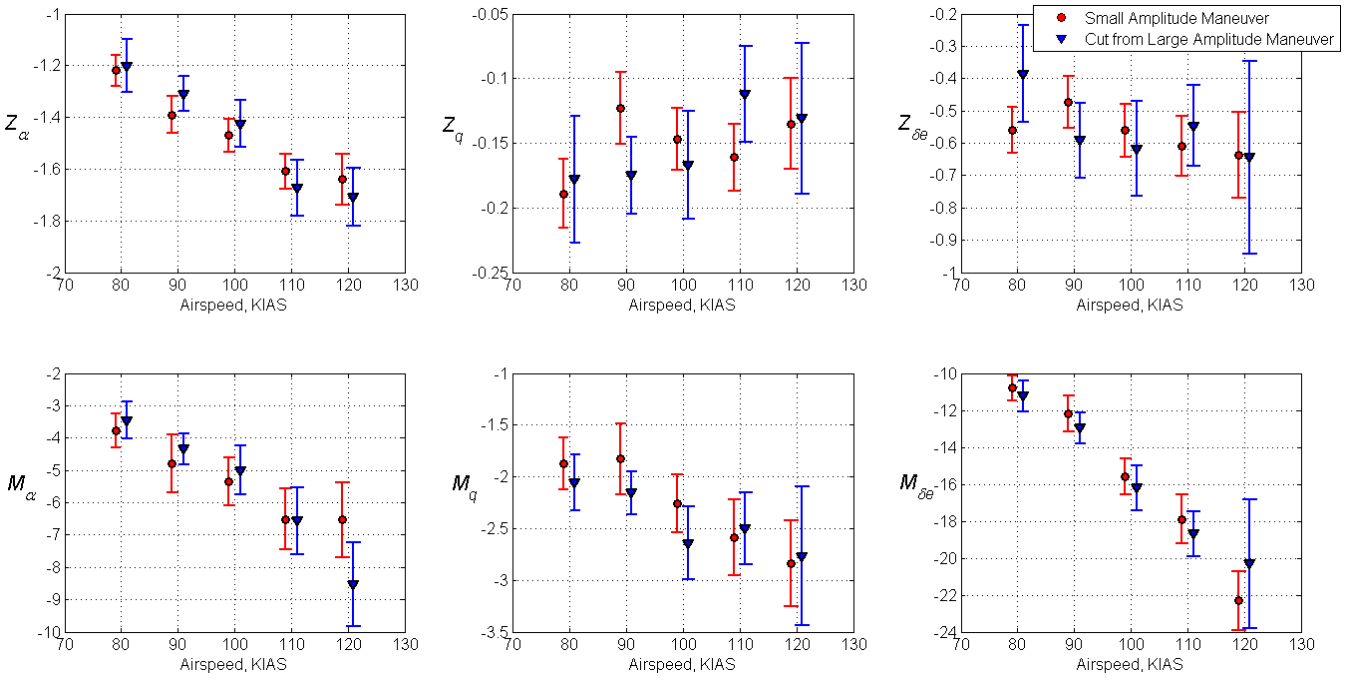


Figure 17. Parameter Estimates Comparison

Figure 17 is the graphical representation of Table 1, which includes comparison plots between the small and large amplitude maneuvers for all six dimensional derivatives that were calculated. The figure shows that many of the estimates from the cut large amplitude maneuver data sets lie within the error bars of the small amplitude maneuvers. The estimates of the cut data sets that do not lie within the error bars of the small amplitude maneuvers share overlapping error bars. This again suggests that large amplitude maneuvers can be used to obtain similar results that would be obtained with small amplitude maneuvers, but in less time.

CONCLUSIONS

System identification is used to determine the aircraft stability and control derivatives from the aircraft equations of motion. Aircraft system identification program, SIDPAC (Ref. 1), was used to calculate the stability and control derivatives estimates by using equation-error in the frequency domain. UTSI's Piper Saratoga was tested using a tone program to cue the pilot for manual control inputs. Small amplitude maneuvers and large amplitude maneuvers were compared using local and global aerodynamic modeling.

The large amplitude maneuvers used to quantify the aerodynamics of the Piper Saratoga were performed using individual doublets at various airspeeds throughout the operational velocity range of the aircraft. The large amplitude maneuver that was performed through stall gives better results in most parameter estimates by a significant margin over the large amplitude maneuver that was done near stall.

Both large amplitude maneuvers investigated the use of a global nonlinear aerodynamic model. Step wise regression identified which nonlinear terms of the model made the most contribution to the aerodynamics. For the large amplitude maneuvers performed on the Piper Saratoga, it was shown that the nonlinear term, α^2, was the only significant nonlinear term. the other nonlinear terms, including q^2 and $\delta_e{}^2$, did not have a significant contribution to the aerodynamic force and moment model.

The parameter estimates obtained from the cut data sets from the large amplitude maneuver show nearly the same result when compared with the parameter estimates from the small amplitude maneuvers, and in most cases they are within the 95 percent confidence interval.

In conclusion, the large amplitude maneuver flight test technique with manual pilot inputs can be applied to produce analogous stability and control derivatives as a small amplitude maneuver. This suggests that stability and control derivatives can be obtained in less time by performing a large amplitude maneuver, and can be done manually without computerized inputs. The time efficiency of the large amplitude maneuver method can be realized in cost savings for the flight test campaign. From the results shown, there was a time savings of fifteen minutes between the large amplitude maneuver and all the small amplitude maneuvers. Further work and research could be conducted applying the same methods and techniques for lateral-directional motion.

REFERENCES

[1]Klein, V. and Morelli, E.A. Aircraft System Identification – Theory and Practice, AIAA Education Series, AIAA, Reston, VA, 2006.

[2]Morelli, E.A. "Efficient Global Aerodynamic Modeling from Flight Data," AIAA 2012-1050, *50th AIAA Aerospace Science meeting,* Nashville, TN, January 2012.

[3]Brandon, J.M. and Morelli, E.A. "Nonlinear Aerodynamic Modeling From Flight Data Using Advanced Piloted Maneuvers and Fuzzy Logic," NASA/TM-2012-217778, October 2012.

[4]Kelly, C.A "System Identification and Parameter Estimation of the Piper PA32-301 Saratoga" Thesis, *University of Tennessee,* Knoxville, TN, December 2006.

[5]Morelli, E.A. "Flight Test Maneuver Design for Efficient Aerodynamic Modeling," AIAA 2011-6672, *AIAA Atmospheric Flight Mechanics Conference,* Portland, OR, August 2011.

[6]Sorensen, T. and Martos, B. "A Comparison between Global and Local Aerodynamic Modeling from Flight Data" AIAA 2013-0472, *51th AIAA Aerospace Science meeting,* Grapevine, TX, January 2013.

[7]Morelli, E.A., "Practical Aspects of the Equation-Error Method for Aircraft Parameter Estimation," AIAA-2006-6144, *AIAA Atmospheric Flight Mechanics Conference*, Keystone, CO, August 2006.

[8]Morelli, E.A. "High Accuracy Evaluation of the Finite Fourier Transform using Sampled Data," NASA TM 110340, 1997.

[9]Kolwyck, J "Simulating the Effects of Outer-Mold-Line Modification on the University of Tennessee Space Institute's Aviation Systems' Piper Navajo Research Aircraft" Thesis, *University of Tennessee,* Knoxville, TN, August 2012.

APPENDIX

Tables

Table 1. Small Amplitude Maneuvers Compared with Cut Data Sets from Large Amplitude Maneuver

Airspeed	Parameter	Small Amplitude Maneuvers			Cut from Large Amplitude Maneuver		
		Estimate	%Error	95% Confidence Interval	Estimate	%Error	95% Confidence Interval
80 KIAS	Z_α	-1.220	2.3	[-1.279 , -1.164]	-1.201	4.3	[-1.304 , -1.097]
	Z_q	-0.189	7.0	[-0.216 , -0.163]	-0.178	13.7	[-0.227 , -0.130]
	$Z_{\delta e}$	-0.560	6.3	[-0.631 , -0.489]	-0.386	19.4	[-0.536 , -0.236]
	M_α	-3.780	7.1	[-4.317 , -3.247]	-3.453	8.4	[-4.030 , -2.877]
	M_q	-1.870	6.6	[-2.112 , -1.618]	-2.059	6.6	[-2.331 , -1.787]
	$M_{\delta e}$	-10.80	3.1	[-11.46 , -10.13]	-11.24	3.7	[-12.07 , -10.40]
90 KIAS	Z_α	-1.390	2.7	[-1.466 , -1.318]	-1.309	2.6	[-1.378 , -1.241]
	Z_q	-0.123	11.4	[-0.151 , -0.095]	-0.175	8.5	[-0.204 , -0.145]
	$Z_{\delta e}$	-0.474	8.5	[-0.555 , -0.393]	-0.592	9.9	[-0.709 , -0.475]
	M_α	-4.790	9.3	[-5.678 , -3.898]	-4.347	5.6	[-4.831 , -3.863]
	M_q	-1.830	9.2	[-2.168 , -1.492]	-2.156	4.9	[-2.366 , -1.946]
	$M_{\delta e}$	-12.20	4.0	[-13.18 , -11.23]	-12.96	3.2	[-13.79 , -12.14]
100 KIAS	Z_α	-1.470	2.1	[-1.528 , -1.406]	-1.425	3.2	[-1.516 , -1.334]
	Z_q	-0.147	8.1	[-0.171 , -0.123]	-0.167	12.6	[-0.209 , -0.125]
	$Z_{\delta e}$	-0.561	7.2	[-0.642 , -0.480]	-0.618	11.9	[-0.765 , -0.471]
	M_α	-5.350	6.9	[-6.086 , -4.614]	-5.000	7.6	[-5.757 , -4.244]
	M_q	-2.260	6.4	[-2.551 , -1.976]	-2.641	6.6	[-2.991 , -2.291]
	$M_{\delta e}$	-15.60	3.1	[-16.57 , -14.62]	-16.20	3.8	[-17.42 , -14.98]
110 KIAS	Z_α	-1.610	2.1	[-1.679 , -1.544]	-1.673	3.2	[-1.780 , -1.567]
	Z_q	-0.161	8.0	[-0.187 , -0.135]	-0.112	16.3	[-0.149 , -0.075]
	$Z_{\delta e}$	-0.609	7.6	[-0.701 , -0.517]	-0.546	11.5	[-0.671 , -0.420]
	M_α	-6.510	7.3	[-7.456 , -5.559]	-6.567	7.8	[-7.594 , -5.541]
	M_q	-2.590	7.0	[-2.949 , -2.222]	-2.500	7.0	[-2.851 , -2.149]
	$M_{\delta e}$	-17.90	3.6	[-19.17 , -16.58]	-18.68	3.2	[-19.89 , -17.48]
120 KIAS	Z_α	-1.640	3.0	[-1.739 , -1.544]	-1.710	3.3	[-1.822 , -1.599]
	Z_q	-0.135	12.8	[-0.170 , -0.101]	-0.131	21.8	[-0.189 , -0.074]
	$Z_{\delta e}$	-0.636	10.4	[-0.768 , -0.503]	-0.644	23.1	[-0.942 , -0.347]
	M_α	-6.530	8.9	[-7.691 , -5.377]	-8.535	7.6	[-9.841 , -7.229]
	M_q	-2.840	7.3	[-3.251 , -2.428]	-2.771	12.1	[-3.442 , -2.100]
	$M_{\delta e}$	-22.30	3.5	[-23.90 , -20.75]	-20.310	8.6	[-23.79 , -16.84]

Table 2. Stepwise regression results, body-axis Z force for a large amplitude maneuver

Step	1			2			3			4			5		
	θ	F_0	r	θ	F_0	r	θ	F_0	r	θ	F_0	r	θ	F_0	r
Z_α	0	–	0.789	-1.408	171.96	0	-2.489	189.79	0	-2.469	224.16	0	-2.187	195.72	0
Z_q	0	–	0.099	0	–	0.067	0	–	0.186	-0.112	10.07	0	-0.174	26.87	0
$Z_{\delta e}$	0	–	0.149	0	–	0.146	0	–	0.057	0	–	0.287	-0.362	17.277	0
Z_α^2	0	–	0.442	0	–	0.493	4.01	43.817	0	4.128	55.546	0	3.465	48.13	0
Z_q^2	0	–	0.175	0	–	0.0027	0	–	0.0037	0	–	0.002	0	–	0.0161
$Z_{\delta e}^2$	0	–	0.182	0	–	0.06223	0	–	0.083	0	–	0.16	0	–	0.0043
PRESS		1.42			0.328			0.16			0.134			0.0988	
PSE		0.023			0.00734			0.0049			0.005			0.0048	
R^2, %		0			78.9			89.31			91.3			93.79	

Step	1			2			3			4			5		
	θ	F_0	r	θ	F_0	r	θ	F_0	r	θ	F_0	r	θ	F_0	r
M_α	0	–	0.313	0	–	0.465	-5.14	39.125	0	-3.999	29.655	0	-10.296	54.212	0
M_q	0	–	0	0	–	0.385	0	–	0.313	-1.667	20.052	0	-1.538	26.061	0
$M_{\delta e}$	0	–	0.713	-13.719	114.37	0	-12.231	156.42	0	-14.059	235.71	0	-12.822	270.85	0
M_α^2	0	–	0.102	0	–	0.211	0	–	0.299	0	–	0.365	22.202	24.705	0
M_q^2	0	–	0.0011	0	–	0.139	0	–	0.0006	0	–	0.0086	0	–	0.009
$M_{\delta e}^2$	0	–	0.471	0	–	0.0083	0	–	0.0203	0	–	0.161	0	–	0.0713
PRESS		105.63			31.142			17.344			11.899			7.743	
PSE		2.19			0.707			0.467			0.409			0.372	
R^2, %		0			71.32			84.66			89.46			93.31	

Table 3. Large Amplitude Maneuver Comparison Near and Through Stall

Parameter	Large Amplitude Maneuver - Near Stall			Large Amplitude Maneuver Though Stall		
	Estimate	% Error	95% Confidence Interval	Estimate	% Error	95% Confidence Interval
Z_α	-2.735	12.9	[-3.440 , -2.030]	-2.187	7.1	[-2.496 , -1.878]
Z_q	-0.114	57.2	[-0.243 , 0.016]	-0.175	19.1	[-0.241 , -0.108]
$Z_{\delta e}$	-0.252	76.3	[-0.637 , 0.133]	-0.362	23.8	[-0.534 , -0.190]
Z_α^2	0.115	30.9	[0.044 , 0.186]	3.465	14.2	[0.043 , 0.078]
M_α	-10.24	18.1	[-13.96 , -6.530]	-10.3	13.4	[-13.06 , -7.531]
M_q	-1.872	18.3	[-2.556 , -1.189]	-1.538	19.4	[-2.134 , -0.942]
$M_{\delta e}$	-14.69	6.9	[-16.72 , -12.66]	-12.82	6.0	[-14.36 , -11.28]
M_α^2	0.602	31.0	[0.228 , 0.975]	22.2	19.9	[0.233 , 0.542]

Derivation of the Equations of Motion from First Principles

An example of the equation of motion derivation in the body axis from first principles. The following example is for the Moment equations

$$\boldsymbol{M} = \frac{\mathrm{d}}{\mathrm{d}t}\left(I\boldsymbol{\omega}\right) \tag{78}$$

$$\boldsymbol{M} = \begin{bmatrix} M_x \\ M_y \\ M_z \end{bmatrix} \qquad I = \begin{bmatrix} I_x & -I_{xy} & -I_{xz} \\ -I_{yx} & I_y & -I_{yz} \\ -I_{zx} & -I_{zy} & I_z \end{bmatrix} \qquad \boldsymbol{\omega} = \begin{bmatrix} p \\ q \\ r \end{bmatrix} \tag{79}$$

Inertia matrix I is symmetric $I_{xy} = I_{yx} = I_{zy} = I_{yz} = 0$

$$I = \begin{bmatrix} I_x & 0 & -I_{xz} \\ 0 & I_y & 0 \\ -I_{zx} & 0 & I_z \end{bmatrix} \tag{80}$$

$$I\boldsymbol{\omega} = \begin{bmatrix} I_x & 0 & -I_{xz} \\ 0 & I_y & 0 \\ -I_{zx} & 0 & I_z \end{bmatrix} \begin{bmatrix} p \\ q \\ r \end{bmatrix} = \begin{bmatrix} I_x p - I_{xz} r \\ I_y q \\ -I_{zx} p + I_z r \end{bmatrix} \tag{81}$$

For rotating axis systems, apply derivative operator, one for rate of change of the vector components in the rotating system and one for the axis system rotation.

$$\frac{\mathrm{d}}{\mathrm{d}t}(\bullet) = \frac{\delta}{\delta t}(\bullet) + \boldsymbol{\omega} \times (\bullet) \tag{82}$$

$$\boldsymbol{M} = \frac{\partial}{\partial t}\left(I\boldsymbol{\omega}\right) + \boldsymbol{\omega} \times \left(I\boldsymbol{\omega}\right) \tag{83}$$

$$\boldsymbol{M} = \left(I\dot{\boldsymbol{\omega}}\right) + \boldsymbol{\omega} \times \left(I\boldsymbol{\omega}\right) \tag{84}$$

$$\begin{bmatrix} M_x \\ M_y \\ M_z \end{bmatrix} = I \begin{bmatrix} \dot{p} \\ \dot{q} \\ \dot{r} \end{bmatrix} + \begin{bmatrix} p \\ q \\ r \end{bmatrix} \times \begin{bmatrix} I_x p - I_{xz} r \\ I_y q \\ -I_{zx} p + I_z r \end{bmatrix} \tag{85}$$

Cross product term

$$\boldsymbol{\omega} \times (I\boldsymbol{\omega}) = \begin{bmatrix} q(-I_{zx} p + I_z r) - r(I_y q) \\ -\left[p(I_{zx} p + I_z r) - r(I_x p - I_{xz} r) \right] \\ p(I_y q) - q(I_x p - I_{xz} r) \end{bmatrix} \tag{86}$$

Matrix product term

$$I\dot{\boldsymbol{\omega}} = \begin{bmatrix} I_x & 0 & -I_{xz} \\ 0 & I_y & 0 \\ -I_{zx} & 0 & I_z \end{bmatrix} \begin{bmatrix} \dot{p} \\ \dot{q} \\ \dot{r} \end{bmatrix} = \begin{bmatrix} I_x \dot{p} - I_{xz} \dot{r} \\ I_y \dot{q} \\ -I_{zx} \dot{p} + I_z \dot{r} \end{bmatrix} \tag{87}$$

Adding terms $(I\dot{\boldsymbol{\omega}}) + \boldsymbol{\omega} \times (I\boldsymbol{\omega})$ together

$$\boldsymbol{M} = \begin{bmatrix} I_x \dot{p} - I_{xz} \dot{r} \\ I_y \dot{q} \\ -I_{zx} \dot{p} + I_z \dot{r} \end{bmatrix} + \begin{bmatrix} q(-I_{zx} p + I_z r) - r(I_y q) \\ -\left[p(I_{zx} p + I_z r) - r(I_x p - I_{xz} r) \right] \\ p(I_y q) - q(I_x p - I_{xz} r) \end{bmatrix} \tag{88}$$

$$\begin{aligned} M_x &= \dot{p} I_x - \dot{r} I_{xz} + qr(I_z - I_y) - pqI_{xz} \\ M_y &= \dot{q} I_y + pr(I_x - I_y) + I_{xz}(p^2 - r^2) \\ M_z &= \dot{r} I_z - \dot{p} I_{xz} + pq(I_y - I_x) + qrI_{xz} \end{aligned} \tag{89}$$

Left hand of the moment equation has a aerodynamics, gravity and propulsion term

$$\boldsymbol{M}_A + \boldsymbol{M}_G + \boldsymbol{M}_T = (I\dot{\boldsymbol{\omega}}) + \boldsymbol{\omega} \times (I\boldsymbol{\omega}) \tag{90}$$

Omit the moment gravity term, as there is no moment as it acts through the center of gravity.

$$\boldsymbol{M}_A + \boldsymbol{M}_T = (I\dot{\boldsymbol{\omega}}) + \boldsymbol{\omega} \times (I\boldsymbol{\omega}) \tag{91}$$

The aerodynamic term is

$$\boldsymbol{M}_A = \bar{q}\, S \begin{bmatrix} b\, C_l \\ \bar{c}\, C_m \\ b\, C_n \end{bmatrix} \tag{92}$$

Propulsion term, assuming that the thrust acts along the x-axis, is

$$hp = \begin{bmatrix} I_p \Omega_p \\ 0 \\ 0 \end{bmatrix} \tag{93}$$

$$\boldsymbol{M}_T = \frac{\mathrm{d}}{\mathrm{dz}}(hp) = \boldsymbol{\omega} \times hp = \begin{bmatrix} \boldsymbol{i} & \boldsymbol{j} & \boldsymbol{k} \\ p & q & r \\ I_p \Omega_p & 0 & 0 \end{bmatrix} = \begin{bmatrix} 0 \\ I_p \Omega_p r \\ -I_p \Omega_p q \end{bmatrix} \tag{94}$$

Now, adding the $\boldsymbol{M}_A$ and $\boldsymbol{M}_T$ terms together gives

$$\begin{bmatrix} M_x \\ M_y \\ M_z \end{bmatrix} = \bar{q}\, S \begin{bmatrix} b\, C_l \\ \bar{c}\, C_m \\ b\, C_n \end{bmatrix} + \begin{bmatrix} 0 \\ I_p \Omega_p r \\ -I_p \Omega_p q \end{bmatrix} = \begin{bmatrix} \bar{q} S b\, C_l \\ \bar{q} S \bar{c}\, C_m + I_p \Omega_p r \\ \bar{q} S b\, C_n - I_p \Omega_p q \end{bmatrix} \tag{95}$$

The components of the equations ($\boldsymbol{M}_A + \boldsymbol{M}_T = \left(I\dot{\boldsymbol{\omega}}\right) + \boldsymbol{\omega} \times \left(I\boldsymbol{\omega}\right)$) are

$$\begin{aligned} M_x &\Rightarrow \bar{q} S b C_l = \dot{p} I_x - \dot{r} I_{xz} + qr\left(I_z - I_y\right) - pq I_{xz} \\ M_y &\Rightarrow \bar{q} S \bar{c} C_m + I_p \Omega_p r = \dot{q} I_y + pr\left(I_x - I_y\right) + I_{xz}\left(p^2 - r^2\right) \\ M_z &\Rightarrow \bar{q} S b C_n - I_p \Omega_p q = \dot{r} I_z - \dot{p} I_{xz} + pq\left(I_y - I_x\right) + qr I_{xz} \end{aligned} \tag{96}$$

Putting the derivatives of the states on the left hand side of the equation

$$\begin{aligned} \dot{p} I_x - \dot{r} I_{xz} &= \bar{q} S b C_l - qr\left(I_z - I_y\right) + pq I_{xz} \\ \dot{q} I_y &= \bar{q} S \bar{c} C_m - pr\left(I_x - I_y\right) - I_{xz}\left(p^2 - r^2\right) + I_p \Omega_p r \\ \dot{r} I_z - \dot{p} I_{xz} &= \bar{q} S b C_n - pq\left(I_y - I_x\right) - qr I_{xz} - I_p \Omega_p q \end{aligned} \tag{97}$$

Equation (97) appears in the body of the thesis, equation (13), assuming longitudinal only, $p = r = 0.$

Figures

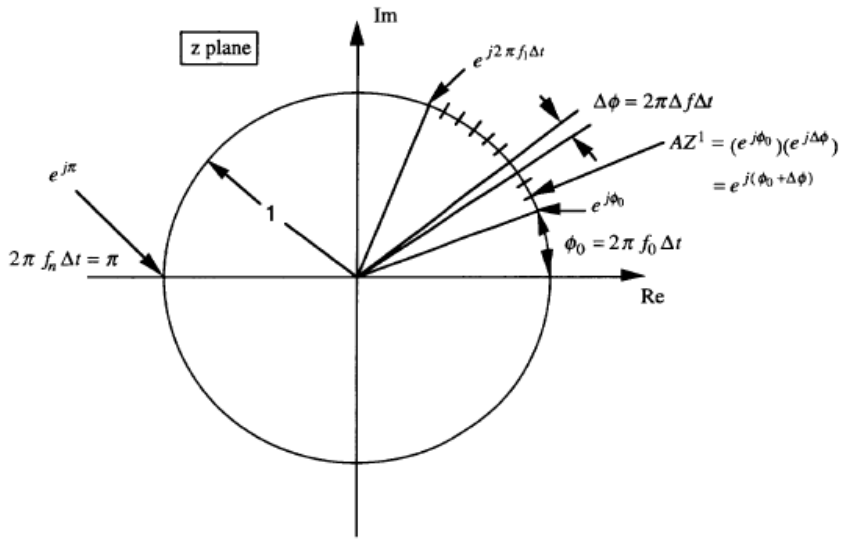


Figure 18. Chirp Z Transform Diagram[8]

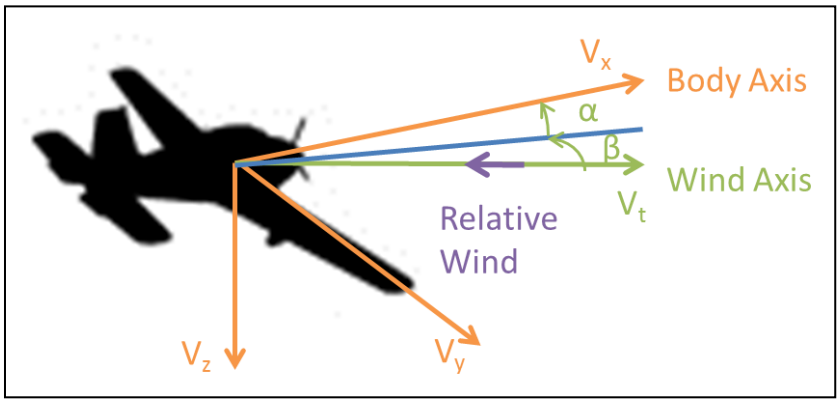


Figure 19. Body and Wind Axis Diagram

(Courtesy of Marie-Michele Siu)

Vita

Toby Earl Sorensen was born on December 7th, 1983 in Kanab, Utah. He grew up on a Ranch in Orderville, Utah. After graduating from Valley High School, Toby served a two year mission for his church in São Paulo, Brazil. In 2006 Toby married Savanna Enid Larson. Toby and Savanna currently have two children: Gaige and Briel. Toby received a Bachelor of Science in Integrated Engineering from Southern Utah University in 2011. During college Toby worked at Lamoureux Group, an engineering firm in Cedar City, Utah. In 2011, he took a Flight Operations internship position at Insitu in Bingen, Washington. Toby currently attends the University of Tennessee Space Institute and works as a Graduate Research Assistant. He will graduate in May 2013 with a degree in Engineering Science and a concentration in Flight Test Engineering. Toby is the president of the UTSI Aero Club and is a member of the AIAA and SFTE. His interests are flight testing, aircraft, building and flying R/C planes, basketball, hiking and spending time with his family. After earning his Masters, Toby hopes to work as a flight test engineer.